2022 44th Annual International Conference of
the IEEE Engineering in Medicine & Biology Society (EMBC)
Scottish Event Campus, Glasgow, UK, July 11-15, 2022

2022 44th Annual International Conference of the IEEE Engineering in Medicine & Biology Society (EMBC) | 978-1-7281-2782-8/22/$31.00 ©2022 IEEE | DOI: 10.1109/EMBC48229.2022.9871675

Analysis of cavitation artifacts in Magnetic Resonance Imaging Thermometry during laser ablation monitoring

Martina De Landro, *Student Member, IEEE*, Francesco La Pietra, Sara Maria Pagotto, Laura Porta, Ilaria Staiano, Céline Giraudeau, Juan Verde, Khalid Ambarki, Leonardo Bianchi, *Student Member, IEEE*, Sanzhar Korganbayev, *Student Member, IEEE*, Henrik Odéen, Benoit Gallix, Paola Saccomandi, *Senior Member, IEEE*

***Abstract*—Magnetic Resonance Thermometry Imaging (MRTI) holds great potential in laser ablation (LA) monitoring. It provides the real-time multidimensional visualization of the treatment effect inside the body, thus enabling accurate intraoperative prediction of the thermal damage induced. Despite its great potential, thermal maps obtained with MRTI may be affected by numerous artifacts. Among the sources of error producing artifacts in the images, the cavitation phenomena which could occur in the tissue during LA induces dipole-structured artifacts. In this work, an analysis of the cavitation artifacts occurring during LA in a gelatin phantom in terms of symmetry in space and symmetry of temperature values was performed. Results of 2 W and 4 W laser power were compared finding higher symmetry for the 2 W case in terms of both dimensions of artifact-lobes and difference in temperature values extracted in specular pixels in the image. This preliminary investigation of artifact features may provide a step forward in the identification of the best strategy to correct and avoid artifact occurrence during thermal therapy monitoring.**

***Clinical Relevance*— This work presents an analysis of cavitation artifacts in MRTI from LA which must be corrected to avoid error in the prediction of thermal damage during LA monitoring.**

I. Introduction

Thermal ablation techniques for cancer treatment are becoming an increasingly valid approach as an alternative to classical surgery, because of their minimally invasive approach [1]. Their principle of operation is based on the selective delivery of thermal energy to cancer cells to cause irreversible damage through the application of extreme temperatures. In laser ablation (LA) the temperature increase is obtained by irradiation of monochromatic laser light which is subsequently absorbed by the tissue target. Magnetic Resonance Thermometry Imaging (MRTI) is used to visualize in real-time the treatment effect enabling accurate intraoperative prediction of the thermal damage induced [2]. The acquired images provide multidimensional measurements of the temperature inside the body, thus allowing the control of the thermal energy radiated by the device in the entire volume for treatment optimization. Proton Resonance Frequency Shift (PRFS) is among the techniques used to obtain MRTI [3]–[5]. PRFS working principle is based on the temperature dependence of proton resonance frequency of tissue protons. MRTI based on the PRF shift is the technique most used in clinics thanks to linear temperature dependency, high precision, and tissue type independence. Nevertheless, thermal maps obtained may be affected by numerous artifacts causing inaccurate temperature measurements, such as artifacts due to motion [6], inhomogeneity of the magnetic field [7], and cavitation [8]. Cavitation is a phenomenon that involves the formation of microbubbles in the areas surrounding the ablation. The occurrence of cavitation during an ablative procedure leads to measurement errors observed as temperature overestimation or underestimation [9]. A dipole-structured artifact was previously observed during high-intensity focused ultrasound and radiofrequency thermal therapies [9][10]. This study is focused on the analysis of the cavitation artifacts occurring on a gelatin phantom undergoing LA in terms of symmetry in space and symmetry of temperature values. MRTI was performed using a 3D EPI protocol based on PRFS. The Comparison among 2 W and 4 W laser power settings was also implemented to observe the effect of laser power on cavitation artifact shape.

II. Materials and Methods

A. Magnetic Resonance Thermometry

The PRFS temperature-dependence is measured in the phase of MRI images. Temperature maps are given by:

* This project has received funding from the European Research Council (ERC) under the European Union's Horizon 2020 research and innovation programme (Grant agreement No. 759159). This work has been supported by the research project "HyperSIGHT" (ID R18SF4YHHS) funded by the Italian Ministry of University and Research (Call FARE Ricerca 2018).

M. De Landro, F. La Pietra, S. M. Pagotto, L. Porta, I. Staiano, L. Bianchi, S. Korganbayev, and P. Saccomandi are with the Department of Mechanical Engineering, Politecnico di Milano, Milano, Italy (martina.delandro@polimi.it, francesco.lapietra@mail.polimi.it, saramaria.pagotto@mail.polimi.it, laura.porta@mail.polimi.it, ilaria.staiano@mail.polimi.it, leonardo.bianchi@polimi.it, sanzhar.korganbayev@polimi.it).

C. Giraudeau, J. Verde, B. Gallix are with the Institute of Image-Guided Surgery, Strasbourg, France (celine.giraudeau@ihu-strasbourg.eu, juan.verde@ihu-strasbourg.eu, benoit.gallix@ihu-strasbourg.eu).

Khalid Ambarki is with Siemens Healthcare SAS, Saint-Denis, France (khalid.ambarki@siemens-healthineers.com).

Henrik Odéen is with the Department of Radiology and Imaging Sciences, University of Utah, Salt Lake City, UT, USA (henrik.odeen@hsc.utah.edu)

P. Saccomandi is with the Department of Mechanical Engineering, Politecnico di Milano, Milano, Italy (corresponding author e-mail: paola.saccomandi@polimi,it).

$$\Delta T = \frac{\varphi - \varphi_{REF}}{\gamma \alpha B_0 TE} \quad (1)$$

The phase image is directly proportional to temperature changes, so it is possible to measure temperature changes by subtracting a reference phase image φ_{REF} obtained prior to the laser procedure, from a phase image obtained during the procedure φ [11]. In (1), γ is the gyromagnetic ratio (Hz/T), α is the temperature-dependent chemical shift coefficient (ppm/°C), B_0 is the main magnetic field (T), and TE is the echo time (s). One of the key properties of the PRFS method, along the absence of tissue-type specificity (except for adipose tissue), is its linear temperature dependency in the range of 15 °C to 100 °C, followed by a good sensitivity and a rapid acquisition of images [6]. These advantages make this method well suited for thermal ablations monitoring. A substantial drawback of the PRFS method is its high susceptibility to movement and to small changes, or drifts, of the B_0 magnetic field [12], which can lead to the appearance of artifacts in the temperature maps. Changes in the local magnetic field may be caused by phenomena occurring during thermal therapy in the tissue, such as cavitation. Cavitation is a phenomenon that involves the formation of microbubbles in the areas surrounding the ablation [9]. The gas bubble formation induces magnetic susceptibility strong contrast producing dipole magnetic field disturbance artifacts. The errors introduced by the B_0 drift can be corrected [3], but artifacts related to motion and bubbles-formation are still a challenge.

B. Experimental setup

A gelatin phantom was used as a target. The gelatin powder (porcine gelatin powder, 200 bloom, LOUIS FRANCOIS, France) was stirred with tap water (10 g/100 mL) for 3h until a homogeneous solution was obtained. Then, the solution was poured into boiling water and stored at 8 °C. LA was performed with a 975 nm laser diode (LuOcean Mini 4, Lumics, Berlin, Germany), delivering the radiation to an MR-compatible fiber applicator with a 365 µm diameter (THORLABS, Dachau, Germany). The laser system was set to deliver power at 2 W and 4 W for 5 minutes. Four ablations were performed in the same gelatin phantom, two for each laser power value. The gelatin phantom was placed in a 1.5 T MRI scanner (MAGNETOM Aera, Siemens Healthineers, Erlangen, Germany). MRI images were acquired with a flexible 4-channel coil and the spine coil integrated into the MRI bed. The flexible coil was positioned for signal reception on the upper side of the entire system. MRTI data was acquired with a prototype 3D segmented EPI sequence in the sagittal orientation, with the following parameters: field of view 300x300 mm², phase resolution 50%, in-plane resolution 1.4 mmx2.8 mm, reconstructed resolution 1.4 mm x1.4 mm, slice thickness 3 mm, 10 slices, TE/TR=13 ms/24 ms, flip angle 10°, EPI factor 7, temporal resolution 3.62 s, 130 repetitions, leading to an overall acquisition times of ~7.8 min. After 5 min of ablation, the cooling phase was also monitored for 2.8 min. Real-time visualization of the thermal maps was performed with Certis Solution software (Certis Therapeutics, France).

C. Data analysis

Image segmentation. The analysis of the artifacts was performed only in the slice closer to the laser applicator for each experiment. This slice was chosen since preliminary investigations showed the largest cavitation artifact and maximum temperature rise in this slice. The artifact in the images was detected using a thresholding technique where the selected slice was manually annotated using GNU Image Manipulation Program. Images manually annotated were used to find the temperature threshold detecting the artifact. The optimal threshold was selected considering the maximum DICE. Then, a single global threshold was obtained averaging among the results obtained in each test for 10-time instants. Two different temperature thresholds were found: -4 ± 1 °C and -5 ± 1 °C for 2 W and 4 W tests, respectively.

Spatial symmetry. After segmenting the artifact in the images, its spatial symmetry was investigated. Considering the double-lobe shape of temperature decrease, also previously observed [9], a horizontal axis of symmetry was drawn starting from the laser tip coordinates which were manually selected. Starting from the axis definition, the areas of the single lobes and the total area of the artifact were computed. In addition, to study the artifact symmetry, the parameter "*Symmetrical ratio*" was defined to quantify the lobes' symmetry with respect to the previously defined axis. This parameter was defined as the percentage ratio between the *symmetric area* and the *total area*. If a pixel of the first lobe and the respective symmetric pixel in the second lobe (see Fig. 4 for examples of first and second lobe) were below the threshold, the *symmetric area* counter was increased by two. Otherwise, the value of the *symmetric area* was not increased.

Symmetry in temperature values. The last step was to evaluate the artifact's symmetry by comparing the temperature evolutions in symmetric pixels with respect to the horizontal axis. For this purpose, three couples of points were selected in both the artifact lobes. These points lay on the axis passing through the center of the smaller lobes and at set distances from the horizontal axis of symmetry: 1/2, 3/4, and 5/6 from the height of the smaller lobe. Once selected the points, the absolute error between the temperature evolution of specular pixels was estimated. Then, one single descriptive value of absolute error was measured by averaging results in the three pixels.

III. RESULTS

A. Image segmentation

Temperature maps were measured in one slice in time during LA for 2 W and 4 W cases in Fig. 1. Slice 7 and Slice 5 were selected and five temporal instants, reported as MRTI measurements, were chosen for the visualization. For both power settings, artifacts appear with a double-lobe shape of negative temperature increase visible in blue with black margins. A bigger artifact is noticeable when the highest power of 4 W is set. Considering that the laser was switched off in correspondence with the 95th measurement, it is worth noticing that the cavitation artifact does not disappear in the cooling phase. Also, the temperature after 95th measurement does not substantially decrease as expected and a temperature error occurrence linkable to cavitation is distinctive.

B. Spatial symmetry

Areas of single lobes and total area estimated in all the tests are reported for 2 W (Fig. 2) and 4 W (Fig. 3). In all the cases, the area is measured as the total number of pixels and shows a trend similar to the temperature one. The maximum area is

estimated at the end of ablation (95th measurement) when also the maximum temperature is expected to occur.

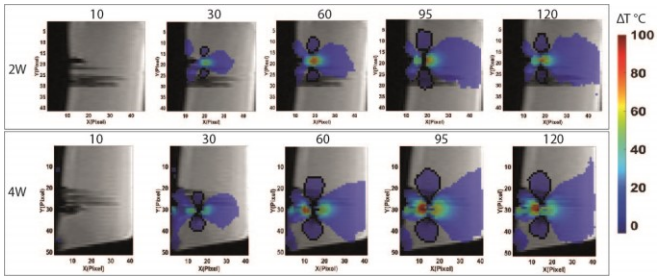

Figure 1. Temperature maps acquired during the gelatin LA at 2 W and 4 W in sagittal orientations reported for 5 temporal instants. Artifacts are visible as negative temperature increase in blue.

After the 95th measurement, the areas start decreasing. Comparing the two power settings, a better reproducibility between the two tests with the same power is measurable in the 2 W case. Also, the two lobes' area (first in blue versus second in orange for each test) is similar when a lower power is set, thus demonstrating also higher symmetry in the 2 W case. The *Symmetrical ratio* shows values varying in the range of 20% to 80% by comparing results of four tests. The estimated value and the effective symmetry between the two lobes was, indeed, more dependent on the structural features and area of the phantom undergoing LA than on set power. Hence, the percentage of *Not symmetrical ratio* was quite different also comparing tests performed with the same power. Furthermore, no specific trend has been noticed over time.

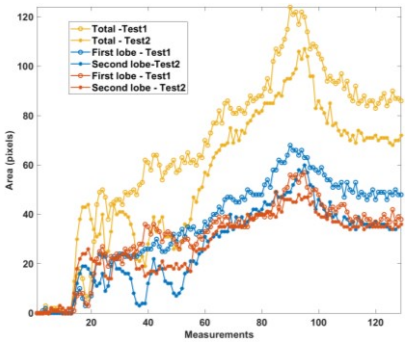

Figure 2. Area of first (blue) and second (orange) lobes and total area (yellow) during gelatin LA for the two tests performed at 2 W.

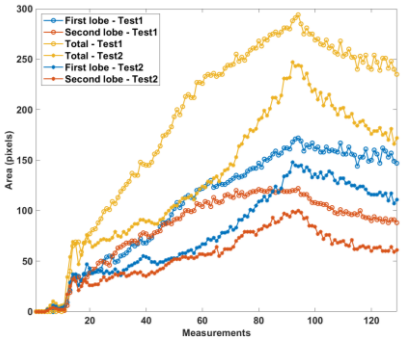

Figure 3. Area of first (blue) and second (orange) lobes and total area (yellow) during gelatin LA for the two tests performed at 4 W.

C. *Symmetry in temperature values*

Temperature evolution in pixels chosen in symmetric positions (as reported in Fig. 4) is shown in Fig. 5.A, 5.B and 5.C. Comparing the values in the couples of pixels, a better match is found for points farther from the laser tip where a higher temperature gradient is measured, and the gelatin is not subjected to structural variation. The temperature mismatch increases with laser ablation progress. Similar behavior is found in all the tests. The highest absolute error of ~18 °C was found in Test1 at 4 W. On the other hand, the tests at 2 W showed a lower maximum error of ~5.5 °C at the 95th measurement (results are reported as average values). The 4 W case demonstrated lower symmetry of the artifact.

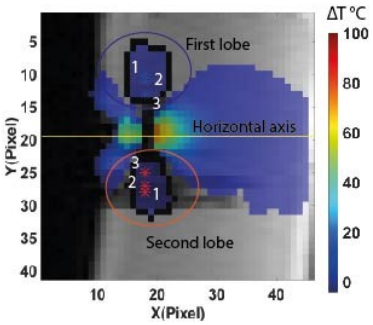

Figure 4. The 3 couple of pixels chosen in specular positions with respect to the horizontal axis (yellow) in the first (blue circle) and second (red circle) lobes.

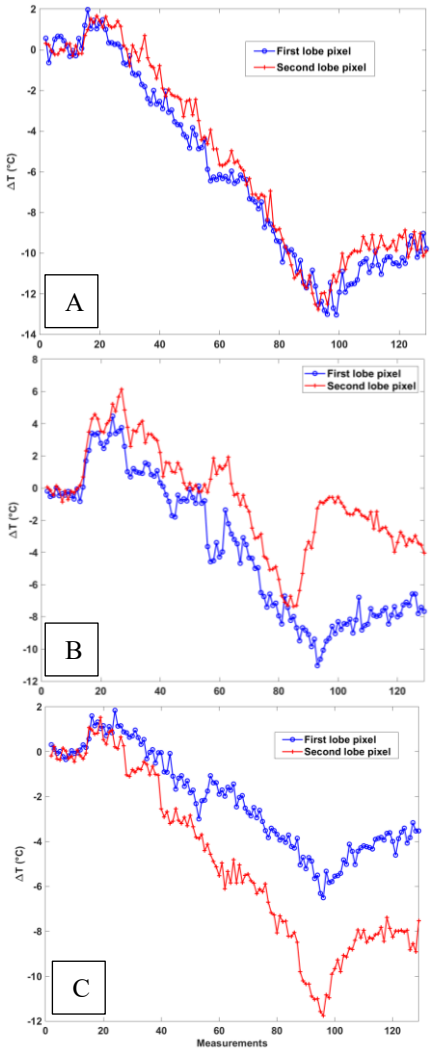

Figure 5. Temporal evolution in the pixels 1 (A), 2 (B) and 3 (C) in Test2 at 2 W. In blue the trend in the first lobe and in red the one in the second lobe.

IV. Discussion & conclusion

MRTI furnishes an attractive approach to monitor in real-time the thermal treatment outcome improving its efficacy. In neurosurgery, MRTI-guided LA is already a clinical alternative for the treatment of brain tumors where PRFS-based protocols are used to provide multidimensional measurements of temperature [13]. Nevertheless, some aspects remain challenging and require further investigation to spread MRTI use in clinics. Among them, PRFS-based MRTI is highly sensitive to changes in the local magnetic field linkable to cavitation phenomena and inducing consistent temperature error. Recently, Munier et al. observed the presence of such artifacts during *in vivo* LA treatments which affected the estimation of thermal damage as well [14]. However, a limited number of works there exist which investigate the cavitation artifact features in space and time. In this study, a preliminary analysis of the cavitation artifact produced during gelatin LA was performed in terms of its symmetrical characteristics. This choice is linkable to the artifact shape which was already observed in previous studies [8]. Symmetrical features of artifact appearing when two different power settings are used, were compared. Firstly, the spatial analysis demonstrated higher symmetry when a 2 W power is set. On the other hand, 4 W leads to bigger artifact' areas and less symmetry compared to 2 W. Hence, if the two areas' lobes differ by ~50 pixels maximum at 4 W, the maximum difference at 2 W is ~12 pixels. As a second step, temperature evolution in specular pixels was compared. In this case, the agreement between the temperature values was higher for pixels further from the laser tip. Also, measuring the absolute temperature error as the difference of the temperature profiles in two specular pixels, a higher value is found as the ablation proceeds with maximum estimation at the end of treatment. For example, in Test 2 at 4 W, absolute temperature error starts from ~2 °C at the beginning of the treatment to reach ~18 °C in the 95th measurements. On the other hand, in Test1 at 2 W, the temperature error shows values from ~1 °C to ~5.5 °C during LA. Comparing the results between the two power settings, also in this case the 2 W demonstrated higher symmetry. Drawbacks of the study can be found in the choice of focusing only on one slice. Also, the analysis is focused only on the two lobes of negative variation of temperature even if a four-lobe pattern in the sagittal slice was previously observed [9]. A more comprehensive study should be performed for the overall artifact shape and in tissue organs. Nevertheless, this work represents the first preliminary analysis of the symmetry of cavitation artifacts appearing in LA. Seeing the temperature error entity and the consequent miscalculation of thermal damage produced, methods to correct susceptibility artifacts should be included in the clinical routine. Simulation-based strategies, mathematical models predicting temperature, or approaches to real-time control microbubbles formation could be used for this purpose [15], [16]. The investigation of the symmetrical features performed in this study would provide additional knowledge of the artifact behavior and of the consequent temperature error, toward the identification of the best strategy to correct and avoid artifact occurrence.

Acknowledgment

The authors would like to acknowledge Dr. John Roberts from the University of Utah for the development and optimization of the 3D EPI prototype, and Certis Therapeutics which provided Certis Solution software used to obtain real-time information during MRT-guided LITT.

References

[1] K. F. Chu and D. E. Dupuy, "Thermal ablation of tumours: biological mechanisms and advances in therapy," *Nat. Rev. Cancer*, vol. 14, no. 3, p. 199, 2014.

[2] V. Rieke and K. B. Pauly, "MR thermometry," *Journal of Magnetic Resonance Imaging*. 2008.

[3] H. Odéen and D. L. Parker, "Magnetic resonance thermometry and its biological applications – Physical principles and practical considerations," *Prog. Nucl. Magn. Reson. Spectrosc.*, vol. 110, pp. 34–61, 2019.

[4] M. De Landro *et al.*, "Fiber bragg grating sensors for performance evaluation of fast magnetic resonance thermometry on synthetic phantom," *Sensors (Switzerland)*, 2020.

[5] M. de Landro *et al.*, "Magnetic resonance-based measurement system: comparison of 2D and 3D echo-planar imaging sequences for thermometry application," in *2021 IEEE International Instrumentation and Measurement Technology Conference (I2MTC)*, 2021, pp. 1–6.

[6] K. K. Vigen, B. L. Daniel, J. M. Pauly, and K. Butts, "Triggered, navigated, multi-baseline method for proton resonance frequency temperature mapping with respiratory motion," *Magn. Reson. Med.*, vol. 50, no. 5, pp. 1003–1010, Nov. 2003.

[7] M. Kangasniemi, R. J. McNichols, J. A. Bankson, A. Gowda, R. E. Price, and J. D. Hazle, "Thermal therapy of canine cerebral tumors using a 980 nm diode laser with MR temperature-sensitive imaging feedback.," *Lasers Surg. Med.*, vol. 35, no. 1, pp. 41–50, 2004.

[8] M. Viallon, S. Terraz, J. Roland, E. Dumont, C. D. Becker, and R. Salomir, "Observation and correction of transient cavitation-induced PRFS thermometry artifacts during radiofrequency ablation, using simultaneous ultrasound/MR imaging," *Med. Phys.*, vol. 37, no. 4, pp. 1491–1506, 2010.

[9] M. Viallon, S. Terraz, J. Roland, E. Dumont, C. D. Becker, and R. Salomir, "Observation and correction of transient cavitation-induced PRFS thermometry artifacts during radiofrequency ablation, using simultaneous Ultrasound/MR imaging," *Med. Phys.*, vol. 37, no. 4, pp. 1491–1506, 2010.

[10] S. M. Sprinkhuizen, M. K. Konings, M. J. van der Bom, M. A. Viergever, C. J. G. Bakker, and L. W. Bartels, "Temperature-induced tissue susceptibility changes lead to significant temperature errors in PRFS-based MR thermometry during thermal interventions.," *Magn. Reson. Med.*, vol. 64, no. 5, pp. 1360–1372, Nov. 2010.

[11] J. Blackwell *et al.*, "Proton Resonance Frequency Shift Thermometry: A Review of Modern Clinical Practices," *J. Magn. Reson. Imaging*, vol. n/a, no. n/a, Nov. 2020.

[12] C. Rosenberg *et al.*, "PRFS-Based MR Thermometry Versus an Alternative T1 Magnitude Method – Comparative Performance Predicting Thermally Induced Necrosis in Hepatic Tumor Ablation," *PLoS One*, vol. 8, no. 10, p. e78559, Oct. 2013.

[13] U. Salem *et al.*, "Neurosurgical applications of MRI guided laser interstitial thermal therapy (LITT)," *Cancer Imaging*, vol. 19, no. 1, p. 65, 2019.

[14] S. M. Munier, A. N. Desai, N. V Patel, and S. F. Danish, "Effects of Intraoperative Magnetic Resonance Thermal Imaging Signal Artifact During Laser Interstitial Thermal Therapy on Thermal Damage Estimate and Postoperative Magnetic Resonance Imaging Ablative Area Concordance.," *Oper. Neurosurg. (Hagerstown, Md.)*, vol. 18, no. 5, pp. 524–530, May 2020.

[15] P. Baron *et al.*, "Correction of proton resonance frequency shift MR-thermometry errors caused by heat-induced magnetic susceptibility changes during high intensity focused ultrasound ablations in tissues containing fat," *Magn. Reson. Med.*, vol. 72, no. 6, pp. 1580–1589, Dec. 2014.

[16] S. Unnikrishnan and A. L. Klibanov, "Microbubbles as Ultrasound Contrast Agents for Molecular Imaging: Preparation and Application," *Am. J. Roentgenol.*, vol. 199, no. 2, pp. 292–299, Aug. 2012.